



Heat transfer in enclosures having a fixed amount of solid material simulated with heterogeneous and homogeneous models

Edimilson J. Braga, Marcelo J.S. de Lemos *

Departamento de Energia—IEME, Instituto Tecnológico de Aeronáutica—ITA, 12228-900 São José dos Campos, SP, Brazil

Received 22 July 2004; received in revised form 21 May 2005

Available online 27 July 2005

Abstract

This work compares two different approaches for obtaining numerical solutions for laminar and turbulent natural convection within a cavity filled by a fixed amount of a solid conducting material. In the first model, a *porous-continuum*, *homogeneous* or *macroscopic* approach is considered based on the assumption that the solid and the fluid phases are observed as a single medium, over which volume-averaged transport equations apply. Secondly, a *continuum*, *heterogeneous* or *microscopic* model is considered to solve the momentum equations for the fluid phase resulting in a conjugate heat transfer problem in both the solid and the void space. In the *continuum* model, the solid phase is composed of square obstacles, equally spaced within the cavity. In both models, governing equations are numerically solved using the finite volume method. The average Nusselt number at the hot wall, obtained from the porous-continuum, *homogeneous* or *macroscopic* model, for several Darcy numbers, are compared with those obtained with the second approach, namely the *continuum* model, with different number of obstacles. When comparing the two methodologies, this study shows that the average Nusselt number calculated for each approach for the same Ra_m differs from each other and that this discrepancy increases as the Darcy number decreases, in the *porous-continuum* model, or the number of blocks increases, in the *continuum* model. Inclusion of turbulent transfer raises Nusselt for both the continuum and the porous-continuum models. A correlation is suggested to modify the macroscopic Rayleigh number in order to match the average Nusselt numbers calculated by the two models for $Ra_m = \text{const} = 10^4$ and Da ranging from 1.2060×10^{-4} to 1.

© 2005 Elsevier Ltd. All rights reserved.

Keywords: Porous media; Heat transfer; Natural convection

1. Introduction

Studies on natural convection in porous enclosures have important applications in engineering and environ-

mental research. Heat exchangers, underground spread of pollutants, environmental control, grain storage, food processing, material processing, geothermal systems, oil extraction, store of nuclear waste material, solar power collectors, optimal design of furnaces, crystal growth in liquids, packed-bed catalytic reactors and nuclear reactor safety are just some examples of applications of this subject of study.

* Corresponding author. Tel.: +55 12 3947 5860; fax: +55 12 3947 5842.

E-mail address: delemos@ita.br (M.J.S. de Lemos).

Nomenclature

c_F	Forchheimer coefficient
c_p	fluid specific heat, J/kg °C
Da_{eq}	equivalent Darcy number using K_{eq} given by Eq. (14); $Da_{eq} = \frac{K_{eq}}{H^2}$
Da	Darcy number using a porous medium permeability K ; $Da = \frac{K}{H^2}$
D_p	square rod size, m
\mathbf{g}	gravity acceleration vector, m/s ²
h	heat transfer coefficient, W/m ² °C
H	square height, m
K_{eq}	equivalent permeability for the continuum model, $K_{eq} = \frac{\phi^2 D_p^2}{120(1-\phi)^2}$; m ²
K	specified permeability used with the porous-continuum model; m ²
k_f	fluid thermal conductivity, W/m °C
k_s	solid thermal conductivity, W/m °C
N	number of obstacles
Nu	$Nu = hH/k_{eff}$, Nusselt number
Pr	$Pr = \nu/\alpha_{eff}$, Prandtl number
Ra	$Ra = \frac{g\beta H^3 \Delta T}{\nu_f \alpha}$, fluid Rayleigh number
Ra_ϕ	$Ra_\phi = \frac{g\beta_\phi H^3 \Delta T}{\nu_f \alpha_{eff}}$, volume-averaged Rayleigh number
Ra_m	$Ra \cdot Da_{eq} = Ra_\phi \cdot Da$, Darcy–Rayleigh number
T	temperature, °C

\mathbf{u}	microscopic velocity, m/s
\mathbf{u}_D	Darcy or superficial velocity (volume average of \mathbf{u})

Greek symbols

α	fluid thermal diffusivity, m ² /s
β	fluid thermal expansion coefficient, 1/K
ΔV	representative elementary volume, m ²
ΔV_f	fluid volume inside ΔV
μ	fluid dynamic viscosity, N s/m ²
ν	fluid kinematic viscosity, m ² /s
ρ	fluid density, kg/m ³
ϕ	$\phi = \Delta V_f/\Delta V$, porosity

Special characters

φ	general variable
$\langle \varphi \rangle^i$	intrinsic average
$\langle \varphi \rangle^v$	volume average
${}^i \varphi$	spatial deviation
$ \varphi $	absolute value (Abs)
$\boldsymbol{\varphi}$	general vector variable
φ_{eff}	effective value, $\varphi_{eff} = \phi \varphi_f + (1 - \phi) \varphi_s$
$\varphi_{s,f}$	solid/fluid
$\varphi_{H,C}$	hot/cold
φ_ϕ	macroscopic or porous continuum

The studies on natural convection has received extensive attention since the beginning of the 20th century [1,2]. Furthermore, natural convection in enclosures still attracts attention of researchers and a large number of experimental and theoretical works have been carried out mainly since the early 70s. The compilation and discussion of the main scientific contributions of researchers on understanding of natural convection during the conference on Numerical Methods in Thermal Problems, which took place in Swansea, yielded the classical benchmark of [3] for laminar clear fluid square cavities.

The works of [4–10] have exhibited some important results to the problem of free convection in a rectangular cavity filled with porous media and the monographs of [11] and [12] fully document natural convection in porous media. The recent work of [13], concerned a numerical study of the steady state free convection flow in rectangular and oblique cavities filled with homogeneous porous media using a nonlinear axis transformation. In the mentioned work, Darcy momentum and energy equations are solved numerically using the (ADI) method.

Macroscopic transport modeling of incompressible flows in porous media has been based on the volume-average methodology for either heat [14] or mass trans-

fer [15–17]. In turbulent flows, when time fluctuations of the flow properties are also considered, in addition to spatial deviations, there are two possible methodologies to follow in order to obtain macroscopic equations: (a) application of time-average operator followed by volume-averaging [18–21], or (b) use of volume-averaging before time-averaging is applied [22–24]. However, both sets of macroscopic mass transport equations are equivalent when examined under the recently established *double decomposition* concept [25–28]. Such development, which was initially developed for only the flow variables, has been extended to heat transfer in porous media where both time fluctuations and spatial deviations were considered for temperature and velocity [29,30]. Further, a consistent program of systematic studies based on the *double-decomposition theory* for treating turbulent buoyant flows [31,32], mass transfer [32], non-equilibrium heat transfer [34] and double diffusion [35], in addition to a general classification of models [36], have been published. Recently, the problem of treating interfaces between a porous medium and a clear region, considering a diffusion-jump condition for the mean [37,38] and turbulence fields [39], have also been investigated under the concept first proposed by [25–28].

Studies considering the distribution of a fixed amount of solid material inside an enclosure for laminar buoyancy driven flows can be found in [40] for the case of a single conducting square solid located at the center of a square cavity. The work of [41] also considered the heat transfer from within a fluid filled enclosure with thermal energy being generated by discrete, disconnected solid bodies. Later, in [42], a study in which the *continuum* and the *porous-continuum* models were compared for natural laminar convection in a non-homogeneous differentially heated enclosure, without heat generation, was documented. In the work of [43] an extension of the work performed by [41] was carried out. Studies on flow around circular rods in heated cavities have also been published [44]. Finally, in [45,46], the effects of distributing a fixed amount of solid material inside a porous medium enclosure on the heat transfer process were recently studied.

Motivated by the foregoing, this work presents numerical solutions for steady laminar and turbulent natural convection within a square cavity filled by a fixed amount of solid conducting material. The solid phase is composed by square obstacles, equally spaced within the cavity. Heat transfer across the cavity is simulated using two models. The first model consists in a conjugate heat transfer problem in which governing equations are separately solved for the fluid and solid phases. This approach is known as *continuum*, *heterogeneous* or *microscopic* model. The word “continuum” is employed with the idea of expressing the continuity of both media (solid and fluid), “heterogeneous” emphasizes the two phases considered and “microscopic” identifies the use of local transport equations. For simplicity, this model shall be only referred to as *continuum* from now on.

In the second approach, the cavity is supposed to be completely filled with a porous material instead, having the same quantity of solid material used in the first model. This second approach is recalled as *porous-continuum*, *homogeneous* or *macroscopic* approach. Likewise, the expression “porous-continuum” reflects the use of up-scaling techniques, “homogeneous” indicates that only one phase is considered and “macroscopic” is associated with the application of the volume-averaging operator to the governing equations. Here, also for simplicity, only *porous-continuum* is used to refer to such model. The objective herein is to compare the average Nusselt number calculated by the two models.

For designing engineering systems that would resemble the arrangement of the present analysis, considering an enclosure with distribution of a fixed amount of solid material, the use of a simpler *porous-continuum* model, instead of applying costly and memory demanding distributed flow calculations (*continuum* approach), could benefit the overall design process if repetitive calculations are necessary in order to obtain initial engineering

estimates. Thus, the contribution herein is based on evaluating the use of simpler porous media models when simulating more complex *continuum* models for complex physical systems.

2. The problem considered

As explained above, this work performs heat transfer calculations in cavities containing a fixed amount of solid material. While maintaining the same overall volume, the morphology, shape and distribution of the solid phase within the cavity may differ from case to case. If one associates a permeability to such systems, its value will be different depending on how easy the fluid is able to flow through the solid matrix within the cavity. Also, different fluids are characterized by distinct properties such as the thermal expansion coefficient β . Fig. 1a illustrates situations considering cavities saturated with distinct fluids (different β) with the solid material of different morphology, size and distribution (distinct permeability).

To analyze such an arrangement, the *continuum* model is here employed, in which the flow equations are solved within the void (fluid) space. More specifically, the problem here investigated is schematically presented in Fig. 1b. The corresponding computational grid is presented in Fig. 1c and refers to a square cavity of side $H = 1$ m. In the continuum model, the cavity is partially filled with a fixed amount of solid conducting material, in the form of square obstacles of size D_p that is equally distributed within the cavity. Also, the cavity is isothermally heated from the left, with temperature T_H prevailing over that side, and cooled from the opposing surface, where a constant temperature T_C is maintained. The horizontal walls are kept insulated.

On the other hand, the same physical system of Fig. 1a was also treated as a permeable structure (Fig. 1d), having the same void-to void-plus-solid ratio, or porosity ϕ . In this case, the *porous-continuum* model was applied, in which the flow properties are integrated over a representative elementary volume. The corresponding computational grid is presented in Fig. 1e.

3. Governing equations and numerics

3.1. Continuum model solution

As mentioned before, the *continuum* model solves the local momentum equation within the fluid phase and resolves a conjugated heat transfer problem in both the solid and the void space. Standard equations for this model are available in textbooks on fluid mechanics and heat transfer, and for that they need not to be repeated here. However, it is interesting to point out that

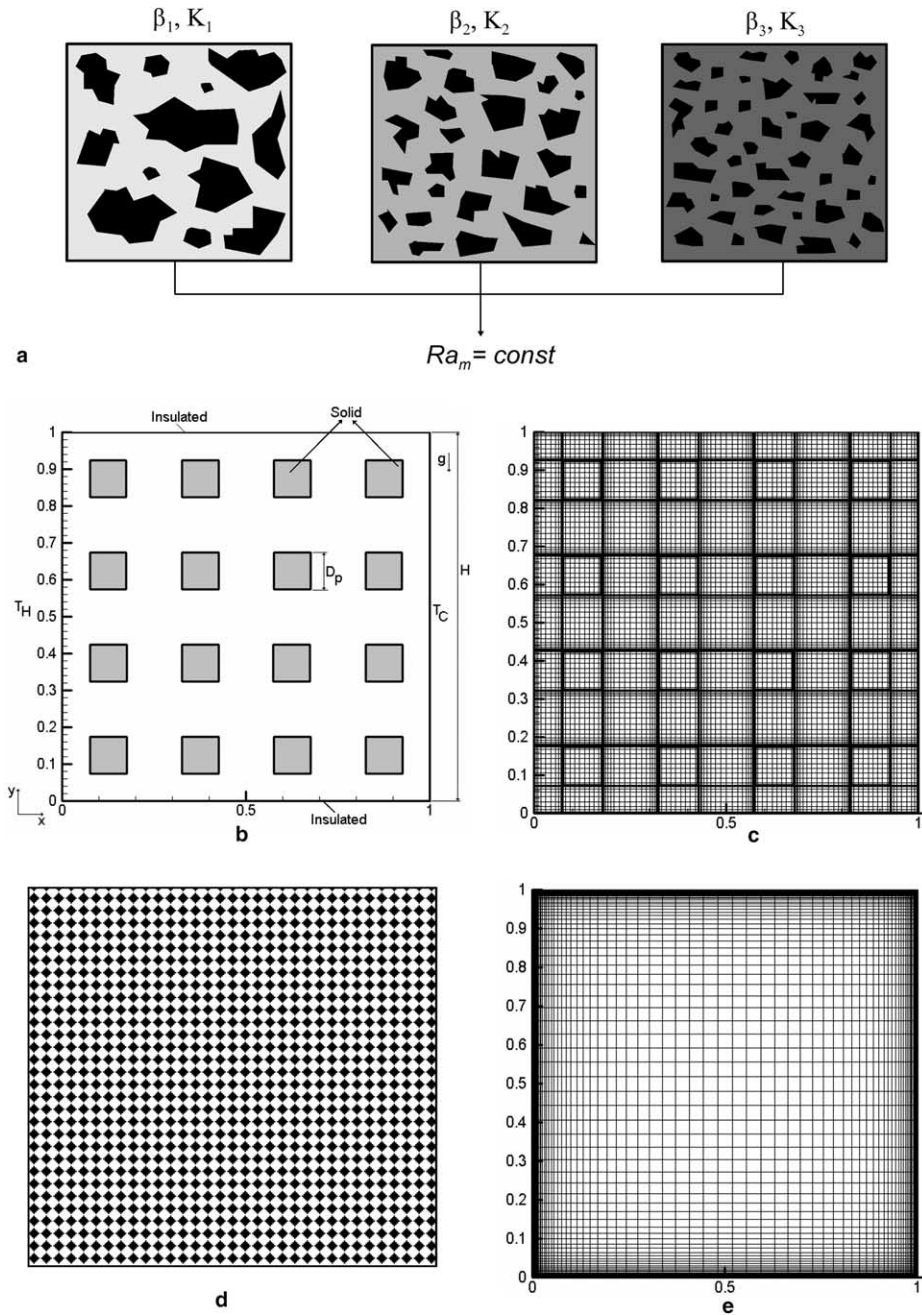


Fig. 1. Physical systems: cavities with different fluids in distinct media (a); continuum model: cavities with distributed solid material (b) and corresponding grid (c); porous continuum model: porous cavity (d) and corresponding grid (e).

the square blocks inside the cavity participate in the momentum transfer through their fluid–solid interfaces, over which, in turn, the no-slip condition was applied. The blocks are heat conducting and the energy balance equation valid inside them is given by

$$k_s \nabla^2 T = 0 \tag{1}$$

3.2. Porous-continuum model solution

In a series of papers, de Lemos and co-workers [25–39] have systematically developed a macroscopic turbulence model for highly porous, highly permeable media. For simplicity, a laminar version of the governing equation set is presented below. Turbulent flow equations are

fully documented in [25–39], and for that they need not to be repeated here. Basically, for porous media analysis, macroscopic form of the governing equations is obtained by taking the volumetric average of the entire equation set. In that development, the porous medium was considered to be rigid and saturated by an incompressible fluid.

The intrinsic average operator is defined by

$$\langle \phi \rangle^i = \frac{1}{\Delta V_f} \int_{\Delta V_f} \phi \, dV \tag{2}$$

where ΔV_f is the volume of fluid phase of the representative elementary volume, over which the integration takes place [16]. For steady state laminar flow the equations take the form:

$$\nabla \mathbf{u}_D = 0 \tag{3}$$

$$\rho \left[\nabla \left(\frac{\mathbf{u}_D \mathbf{u}_D}{\phi} \right) \right] = -\nabla(\phi \langle p \rangle^i) + \mu \nabla^2 \mathbf{u}_D - \left[\frac{\mu \phi}{K} \mathbf{u}_D + \frac{c_F \phi \rho |\mathbf{u}_D| \mathbf{u}_D}{\sqrt{K}} \right] - \rho \beta_\phi \mathbf{g} \phi (\langle T \rangle^i - T_{ref}) \tag{4}$$

where all physical properties are assumed isotropic, uniform and constant, except the fluid density, ρ , in the buoyancy term which, in turn, is modeled using the Boussinesq–Oberbeck approximation. Also, \mathbf{u}_D is the Darcy velocity defined as $\mathbf{u}_D = \phi \langle \mathbf{u} \rangle^i$, where $\langle \mathbf{u} \rangle^i$ is the intrinsic velocity vector, p is the total pressure and μ is the dynamic viscosity, $\langle T \rangle^i$ and T_{ref} are the intrinsic and the reference temperatures, respectively, and c_F is the Forchheimer coefficient.

The macroscopic energy equation reads,

$$(\rho c_p)_f \nabla \cdot (\mathbf{u}_D \langle T \rangle^i) = \nabla \cdot \{ \mathbf{K}_{eff} \cdot \nabla \langle T \rangle^i \} \tag{5}$$

where, \mathbf{K}_{eff} , given by

$$\mathbf{K}_{eff} = [\phi k_f + (1 - \phi) k_s] \mathbf{I} + \mathbf{K}_{tor} + \mathbf{K}_{disp} \tag{6}$$

is the effective conductivity tensor, \mathbf{K}_{tor} and \mathbf{K}_{disp} are the *tortuosity* and *thermal dispersion* conductivity tensors, respectively. Following [20], determination of \mathbf{K}_{tor} and \mathbf{K}_{disp} can be accomplished by making use of a unit cell subjected to periodic boundary conditions for the flow and a linear temperature gradient imposed over the domain. The conductivity tensors are then obtained directly from the microscopic results for the unit cell. Here, for simplicity, the contributions to heat transfer due to these two mechanisms are neglected.

Focusing now attention to buoyancy effects only, application of the volume average procedure to the clear fluid buoyancy term leads to

$$\langle \rho \mathbf{g} \beta (T - T_{ref}) \rangle^v = \frac{\Delta V_f}{\Delta V} \frac{1}{\Delta V_f} \int_{\Delta V_f} \rho \mathbf{g} \beta (T - T_{ref}) \, dV \tag{7}$$

Expanding the left hand side of (7), the buoyancy term becomes,

$$\langle \rho \mathbf{g} \beta (T - T_{ref}) \rangle^v = \rho \beta_\phi \mathbf{g} \phi (\langle T \rangle^i - T_{ref}) + \underbrace{\rho \mathbf{g} \beta_\phi \phi \langle T \rangle^i}_{=0} \tag{8}$$

where the second term on the r.h.s. is null since $\langle \phi \rangle^i = 0$.

Here, the coefficient β_ϕ is an effective macroscopic or volume-averaged thermal expansion coefficient defined by de Lemos and Braga [31] and Braga and de Lemos [32]. Note that β_ϕ and it is not necessarily equal to the thermal expansion coefficient β . Assuming that gravity is constant over the representative elementary volume, REV, an expression for it based on (8) is given in [31] as,

$$\beta_\phi = \frac{\langle \rho \beta (T - T_{ref}) \rangle^v}{\rho \phi (\langle T \rangle^i - T_{ref})} \tag{9}$$

It is important to emphasize that when $K \rightarrow \infty$ and $\phi = 1$ the equation set above resembles the one applied in the cases of clear (unobstructed) flows.

3.3. Non-dimensional parameter

For the systems in Fig. 1a, here also modeled with the geometry and grid of Fig. 1d and e, the literature has defined a modified Rayleigh number Ra_m in the form [4,5,7–10,13,41–46],

$$Ra_m = Ra Da \tag{10}$$

with

$$Ra = \frac{g \beta H^3 \Delta T}{v_f \alpha_{eff}} \tag{11}$$

$$Da = \frac{K}{H^2} \tag{12}$$

where $\alpha_{eff} = k_{eff}/(\rho c_p)_f$ and H is the size of the square cavity. One can note that Ra , as defined by Eq. (11), is similar to the parameter used in clear (unobstructed) heated cavities when k_{eff} is equal to the fluid thermal conductivity. On the other hand, in Eq. (12) the attribution of a permeability K to a porous structured is common path followed in porous media analysis. Eq. (10) then involves *continuum* properties such as the thermal expansion coefficient for fluid phase β and *porous-continuum* parameters such as permeability K . Here, a different Rayleigh number is associated with heated porous cavities, being defined as,

$$Ra_\phi = \frac{g \beta_\phi H^3 \Delta T}{v_f \alpha_{eff}} \tag{13}$$

where β_ϕ is defined in Eq. (9).

Furthermore, in order to associate a value for an “equivalent” permeability of the arrangement in Fig. 1b, for comparisons with the *porous-continuum* model, the correlation of [47] was applied. That correlation is based on the work of [48] and reads,

$$K_{eq} = \frac{D_p^2 \phi^3}{120(1 - \phi)^2} \quad (14)$$

where D_p , as seen, is the size of the square rods. It is important to note that K_{eq} given by Eq. (14) was proposed for forced flows thorough permeable media and that use of such correlation in buoyancy driven flows might be questionable. Nevertheless, in the absence of better information, this work associates a permeability K_{eq} to the system in Fig. 1b using Eq. (14). This equivalent permeability is used to form an “equivalent” Darcy number,

$$Da_{eq} = \frac{K_{eq}}{H^2} \quad (15)$$

As such, this work is based on the hypothesis that both systems in Fig. 1b and d can be compared if the same Ra_m is applied, or say, $Ra_m = Ra Da_{eq}$ characterizing Fig. 1b was equal to $Ra_m = Ra_\phi Da$ describing Fig. 1d. This imposed condition is therefore,

$$Ra_m = Ra \cdot Da_{eq} = \frac{g\beta H \Delta T K_{eq}}{\nu_f \alpha} \left. \begin{array}{l} \text{continuum model—Fig.1b} \\ = Ra_\phi \cdot Da = \frac{g\beta_\phi H \Delta T K}{\nu_f \alpha_{eff}} \end{array} \right\} \quad (16)$$

Porous-continuum model—Fig.1d

Also, if values for Ra or Ra_ϕ and Da or Da_{eq} are selected while Ra_m is kept constant, a family of curves is obtained as schematically shown in Fig. 2. Each curve in the figure represents distinct systems consisting of possibly different fluids and solid distribution, but all having the same modified Rayleigh number Ra_m (see illustration in Fig. 1a). Considering such premise, the present

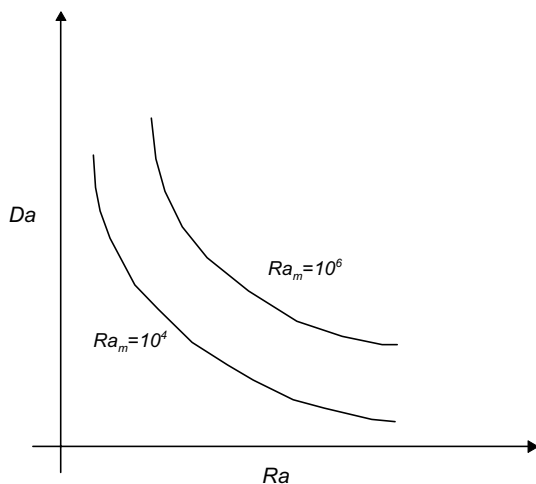


Fig. 2. Family of curves for cavities of Fig. 1a with different fluids in media having the solid phase distributed in different forms and $Ra_m = \text{const}$.

work intends to study a family of cases with different Ra in distinct media (different Da), having all of them the same $Ra_m = 10^4$.

The local Nusselt number on the hot wall for the square cavity at $x = 0$ is defined as,

$$Nu_y = hH/k_{eff}, \quad \therefore Nu_y = \left(\frac{\partial(T)^n}{\partial x} \right)_{x=0} \frac{H}{T_H - T_C} \quad (17)$$

and the average Nusselt number for the *continuum* model (see Fig. 1b and c) is given by,

$$Nu = \frac{1}{H} \int_0^H Nu_y dy \quad (18)$$

For porous cavities computed with the *porous-continuum* model (see Fig. 1d and e), the Nusselt number is here given the symbol Nu_ϕ .

4. Numerical method and solution procedure

The numerical method employed for discretizing the governing equations is the control-volume approach with a generalized grid. The flux blended deferred correction, which combines linearly the Upwind Differencing Scheme (UDS) and Central Differencing Scheme (CDS), was used for interpolating the convective fluxes. The well-established SIMPLE algorithm [51] is followed for handling the pressure–velocity coupling. Individual algebraic equation sets were solved by the SIP procedure of (see [52] for details). Further, concentration of nodal points to walls reduces eventual errors due to numerical diffusion which, in turn, are further annihilated due to the hybrid scheme here adopted.

5. Results and discussion

5.1. Grid independence studies

In order to guarantee grid independent solutions, runs for *porous-continuum* model were also performed with 110×110 control volumes, in addition to 80×80 mesh, in a stretched grid for $Ra_m = 10^4$. The difference of the averaged Nusselt number at the hot wall between these two meshes was smaller than 1%. Therefore, the 80×80 mesh was found to be refined enough near the walls to capture the thin boundary layers that appear along the vertical surfaces. The use of a stretched grid rather than a uniform one is due to the fact that a uniform grid will require several grid points in order to guarantee a first grid point closer enough to the wall to capture the thin boundary layer that appears along the heated walls, mainly for turbulent flows.

For the *continuum* model and for the most stringent case simulated, i.e., $N = 256$ obstacles, a stretched grid

with 151×151 nodes yielded average Nusselt numbers less than 1% different from those obtained when using a grid size of 117×117 stretched nodes. In spite of such small difference, all results herein were computed with the finer 151×151 stretched grid for conservativeness and accuracy enhancement.

5.2. Velocity and temperature fields

First, to validate the *continuum* approach, runs were performed for a clear (of obstacles) cavity and compared with other values from the open literature. Present results were summarized in Table 1 and show good agreement with those obtained from other sources. A case with a single conducting square solid located at the center of the cavity was also performed showing good agreement with those summarized in Table 2.

As said, the main idea of this work is to compare heat transfer simulations in a porous square cavity using the *porous-continuum* and the *continuum* models with several obstacles. Comparisons are based on similar conditions in order to verify if the two models yield equivalent values for the overall Nusselt numbers. As mentioned, runs for *continuum* model solution were performed with a 151×151 control volumes in a stretched grid shown in Fig. 1c. For the sake of comparison of the two models, all calculations were made with $Ra_m = Ra$ $Da = 10^4$. For the continuum model, a Darcy number is associated with the flow in the arrangement of Fig. 1b with a per-

meability K calculated by expression (14), using for D_p the size of the square rod.

As such, when the number of blocks N in the cavity is increased while keeping the overall solid-to-void ratio (equivalent to a constant porosity cavity case), a reduced value of the square rod size D_p yield different K_{eq} values, according to (14), implying in distinct Da_{eq} numbers (see Eq. (12)). However, looking back at Fig. 2 and remembering the definition of Ra (Eq. (11)), for different Darcy numbers one has to modify Ra in order to keep Ra_m fixed at 10^4 . One way to accomplish this is to modify the numerical value of coefficient β in Eq. (11), assuming that a different fluid is being computed for all point laying in the same curve in Fig. 2. One could also modify H , ρ , ΔT or another variable composing Ra . This work used several pairs of values for K and β so that the corresponding Ra and Da were such that their product would yield always $Ra_m = 10^4$. Therefore, coefficients β and K are the variables to be modified in order to maintain Ra_m constant and all cases here analyzed.

It is also interesting to note that when $Da = 1$, Ra_m calculated for the *continuum* model reduces to Ra , similar to the one used for clear (unobstructed) fluid cavities. For that, also shown with this set of results are calculations with the *porous-continuum* model with $Da = 1$ (high permeability K) and $\phi = 0.998$ (high porosity) in order to simulate a clear fluid cavity, which, in turn, would correspond to the case of having no obstacle at all ($N = 0$). In fact, a cavity filled with a porous material with $Da = 1$ and $\phi = 0.998$ is analogous to a continuum model solution with a very small obstacle in its center, which does not contribute effectively to the heat transfer process [45]. Indeed, the difference between the average Nusselt number calculated with the two models, for clear cavity ($N = 0$) and porous cavity with $Da = 1$ and $\phi = 0.998$, is less than 3%, indicating that a porous-continuum model will reproduce a clear fluid cavity solution when appropriate parameters are set in Eqs. (3)–(5). Also, solid obstacles in the cavity yield an overall cavity porosity $\phi = 0.84$ (unless otherwise noted). The fluid Prandtl number and the conductivity ratio between the solid and fluid phases were assumed to be equal to one. Table 3 summarizes the parameters used in the calculations.

Figs. 3 and 4 show the streamlines and isotherms, respectively, for the heterogeneous system of Fig. 1a with several obstacles and equivalent Da ranging from 1 to 1.2060×10^{-4} , $Ra_m = 10^4$, $\phi = 0.84$ and $k_s/k_f = 1$.

Table 1

Average Nusselt numbers for buoyancy-driven laminar flow in clear cavities; $10^4 < Ra < 10^8$, $Pr = 0.71$ (unless otherwise noted)

Ra	10^4	10^5	10^6	10^7	10^8
de Vahl Davis, 1983, [4]	2.243	4.519	8.800	–	–
House et al, 1990, [36]	2.254	4.561	8.923	–	–
Merrikh and Lage, 2004, [45]	2.244	4.536	8.860	16.625	31.200
Kalita et al., 2001, [54]	2.245	4.522	8.829	16.52	–
Lage and Bejan, 1991, [55], $Pr = 1$	–	4.9	9.2	17.9	31.8
Present results, $Pr = 1$	2.249	4.575	8.918	16.725	30.642

Table 2

Average Nusselt number for cavity with a single conducting solid at the center; $Ra = 10^5$, $Pr = 0.71$ (unless otherwise noted)

Ra	D_p	k_s/k_f	House et al, 1990, [36]	Merrikh and Lage, 2004, [45]	Present results $Pr = 1$
10^5	0.5	0.2	4.624	4.605	4.667
10^5	0.5	5.0	4.324	4.280	4.375

Table 3
Parameters used in the arrangement of Fig. 1b for the *continuum* level

$Pr = 1$, equivalent $\phi = 0.84$, $Ra_m = Ra Da = 10^4$, $k_s/k_f = 1$			
$Da = Da_{eq}$ (K_{eq} from (14))	Ra	D_p [m]	$N =$ number of obstacles
Porous cavity with $Da = 1$ and $\phi = 0.998$	$Ra_\phi = Ra = 10^4$ ($\beta_\phi = \beta = 0.001$)	0.022	Equivalent to 0
Clear cavity	10^4	0	0
0.3087×10^{-1}	0.0324×10^7	0.400	1
0.7717×10^{-2}	0.1295×10^7	0.200	4
1.9290×10^{-3}	0.5000×10^7	0.100	16
0.4823×10^{-3}	2.0734×10^7	0.050	64
1.2060×10^{-4}	8.2918×10^7	0.025	256

Figs. 5 and 6 show corresponding results, i.e., same Ra_m , ϕ , Pr and ratio k_s/k_f , for a square cavity completely filled by a porous material. Results in Figs. 3 and 4 are computed with the *continuum* approach whereas Figs. 5 and 6 made use of the *porous-continuum* earlier described.

Comparing Figs. 3a and 5a one can see that clear cavity flow is reproduced in both models if appropriated parameters are set, or say, $N = 0$ (continuum model with no obstacle or clear cavity flow) or $Da = 1$ and $\phi = 0.998$ (highly permeable and highly porous cavity). The same comparisons hold for the thermal field (see Figs. 4a and 6a).

Fig. 3 shows that, in comparison with corresponding cases run with the porous-continuum model, Fig. 5, the higher the number of obstacles inside the clear cavity, the higher the similarity of the flow pattern between the two approaches, i.e., the porous-continuum and the continuum solutions resemble each other for greater values of N (see Figs. 3f and 5f). In other words, the porous-continuum model seems to be more representative of reality when the number of obstacles inside the cavity is higher, which, in turn, correspond to lower permeability cases. Further, Fig. 4 shows that, the higher the number of obstacles, the higher the stratification of the thermal field. This characteristic is also observed for the isotherms of the porous-continuum model, Fig. 6.

Fig. 5 also indicates that the recirculation intensity increases as the medium permeability decreases and the flow patterns comprises primarily cells of relatively high velocity, which circulate around of the entire cavity. However, the secondary recirculation that appears in the center of the cavity, for the higher Darcy numbers analyzed, tends to disappear as the permeability decreases. In a similar way, the temperature gradients are stronger near the vertical walls, but decrease at the center. Fig. 6 shows that the isotherms tend to stratification as Da is decreased, i.e., as the medium permeability is decreased.

According to [45], as the number of square rods increases, and their size becomes reduced, the flow tends to migrate away from the wall towards the center of the cavity. This phenomenon is seen in [45] as a re-

sponse of the system due to the increasing flow resistance closer to the solid wall, as the obstacles get closer to the solid surface.

Further, the available literature shows that for the non-Darcy region in a porous cavity, [32,53], fluid flow and heat transfer depend on the fluid Rayleigh number, Ra , and on the Darcy number, Da , when other parameters, such as porosity, Prandtl number, and conductivity ratio between the fluid and solid matrix, are held constant. In [32] it was shown that for a fixed Ra_m , the lower the permeability (lower Da), the higher the average Nusselt number at the hot wall. It then looks evident that different combinations of Ra and Da yields different heat transfer results, even when Ra_m is the same. The increasing of the fluid Rayleigh number increases the natural convection inside the enclosure. For a fixed Ra_m , a higher fluid Rayleigh number is associated with a less permeable media (i.e. lower Darcy number).

To further validate the present porous-continuum approach, runs were performed for a square cavity totally filled with porous material and results were compared with other values from the open literature. Calculations in [32] made use of the same numerical procedure here exploited. Their results are summarized in Table 4, showing good agreement with several other authors.

5.3. Turbulent field

The set of macroscopic equations used to perform turbulent model solutions, fully documented in [25–30], was extended to natural convection in [31,32] and for that they need not to be repeated here. Turbulent model solutions were performed in the same grids used for laminar model solutions. The stretched grid here adopted is refined enough to capture the thin boundary layer that appears along the heated walls.

Table 5 shows laminar and turbulent average Nusselt numbers for the continuum and porous-continuum models for $0.7717 \times 10^{-2} < Da < 0.4823 \times 10^{-3}$, $Pr = 1$, $\phi = 0.84$, $Ra_m = 10^6$ and $k_s/k_f = 1$. According to Table 5, in both laminar and turbulent solutions a macroscopic model (Nu_ϕ) underestimates the value of Nu

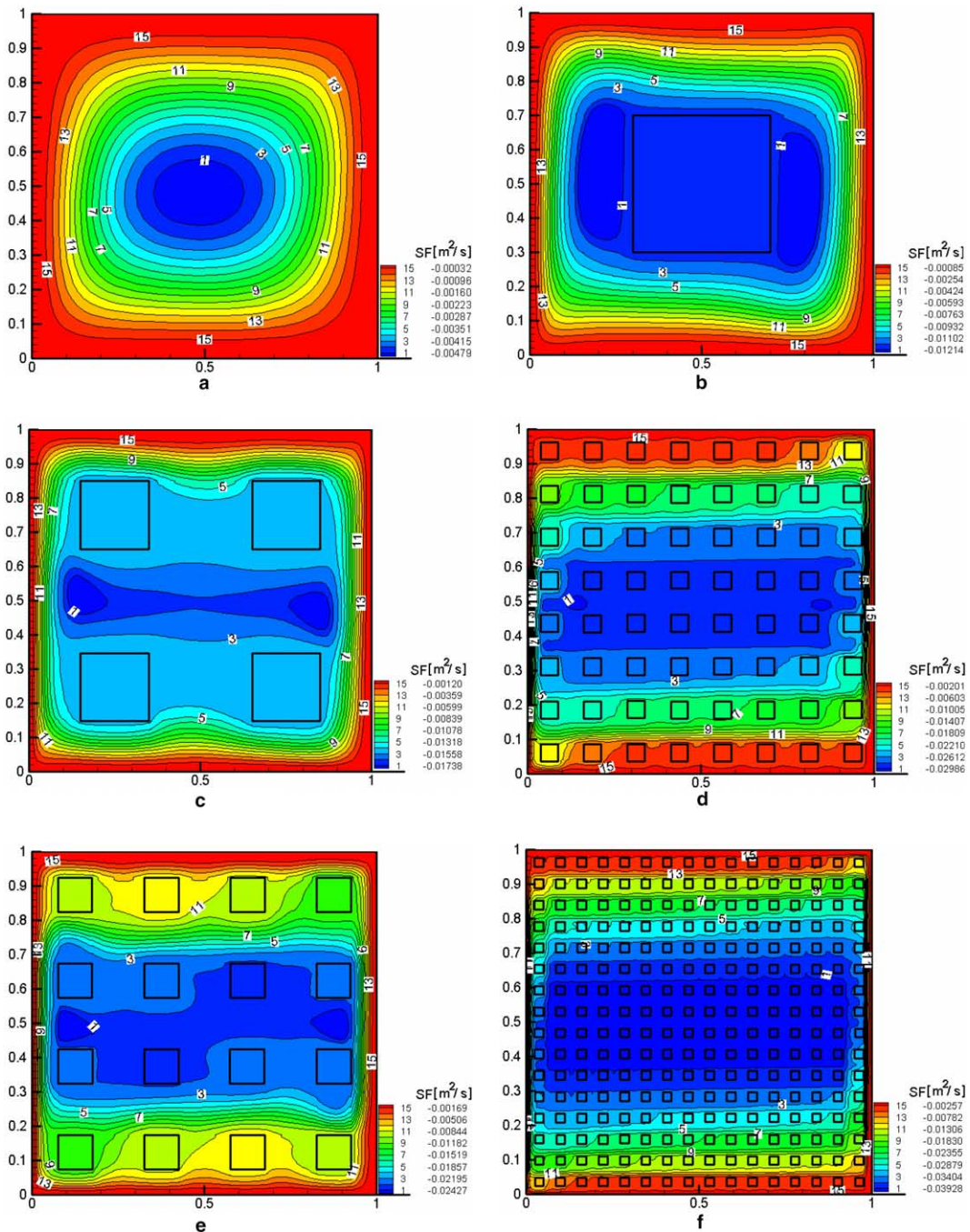


Fig. 3. Streamlines for continuum model solution, $\phi = 0.84$, $Pr = 1$, $k_s/k_f = 1$, $Ra_m = 10^4$: (a) $Da = 1$, $N = 0$, (b) $Da = 0.3087 \times 10^{-1}$, $N = 1$, (c) $Da = 0.7717 \times 10^{-2}$, $N = 4$, (d) $Da = 1.929 \times 10^{-3}$, $N = 16$, (e) $Da = 0.4823 \times 10^{-3}$, $N = 64$ and (f) $Da = 1.206 \times 10^{-4}$, $N = 256$.

and such discrepancy increases as the number of blocks N increases. For laminar solution and $N = 4$ (see Table 5), Nu_ϕ is $(27.8 - 32.9)/32.9 \times 100 = -15.5\%$ lower than Nu and for $N = 64$ such decrease is $(48.3 - 66.7)/$

$66.7 \times 100 = -27.6\%$. The same trend can be observed when turbulence is included, being $Nu_\phi/Nu = (30.73/32.9) = 0.93$ for $N = 4$ and $(62.2/70.8) = 0.88$ when $N = 64$.

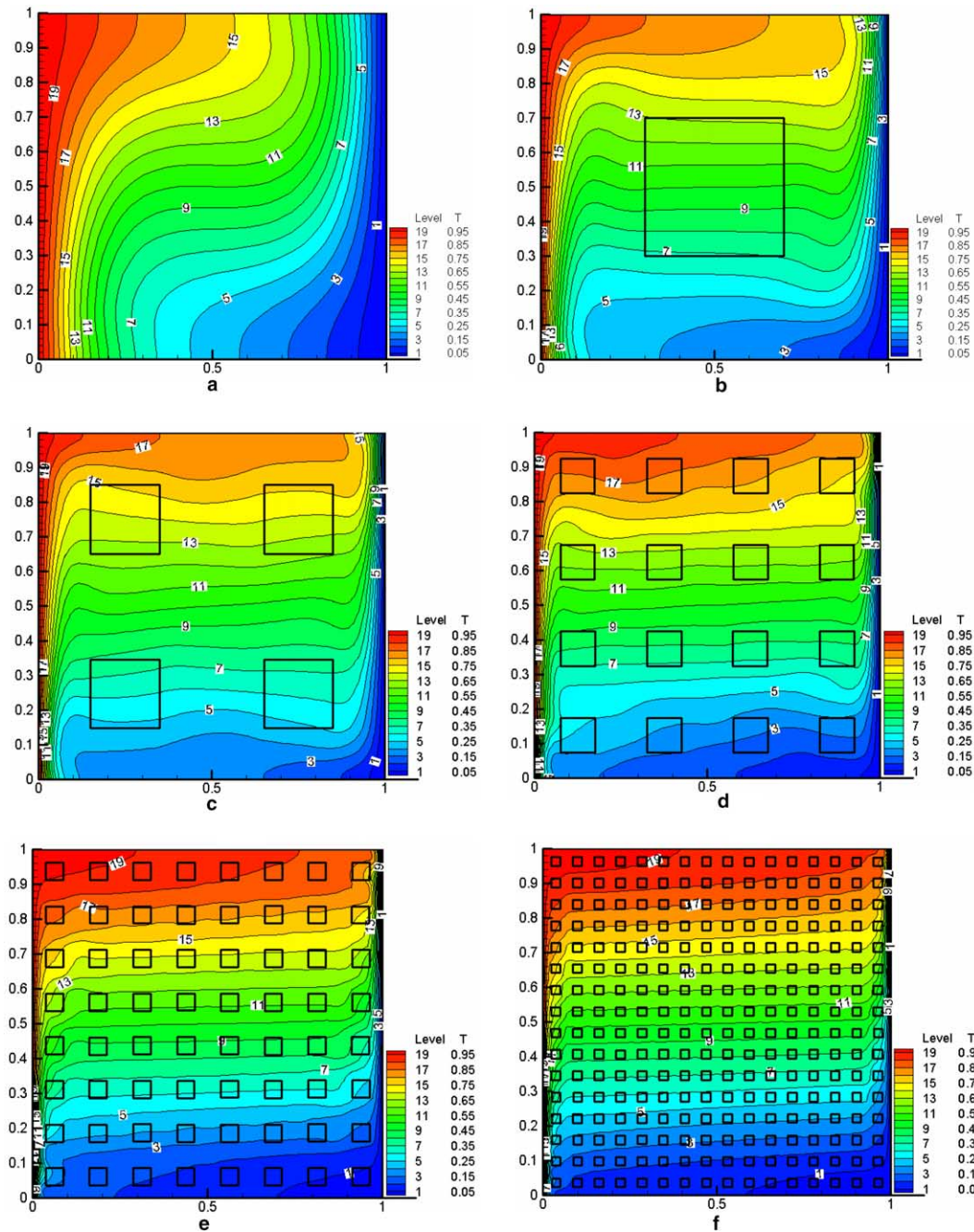


Fig. 4. Isotherms for continuum model solution, $\phi = 0.84$, $Pr = 1$, $k_s/k_f = 1$, $Ra_m = 10^4$: (a) $Da = 1$, $N = 0$, (b) $Da = 0.3087 \times 10^{-1}$, $N = 1$, (c) $Da = 0.7717 \times 10^{-2}$, $N = 4$, (d) $Da = 1.929 \times 10^{-3}$, $N = 16$, (e) $Da = 0.4823 \times 10^{-3}$, $N = 64$, and (f) $Da = 1.206 \times 10^{-4}$, $N = 256$.

Also, both the *continuum* and the *porous continuum* models give higher values for the Nusselt number when turbulence is considered. Further, macroscopic solutions are seen to be more sensitive to the inclusion of a turbulence model (see [32] for details), and this sensitivity in-

creases with the number of blocks N . When $N = 4$, inclusion of turbulence in the calculations rises Nu_ϕ by $(30.7 - 27.8)/27.8 \times 100 = +10.4\%$ and for $N = 64$ Nusselt will be elevated by $(62.2 - 48.3)/48.3 \times 100 = +28.6\%$. On the other hand, turbulent solution using the

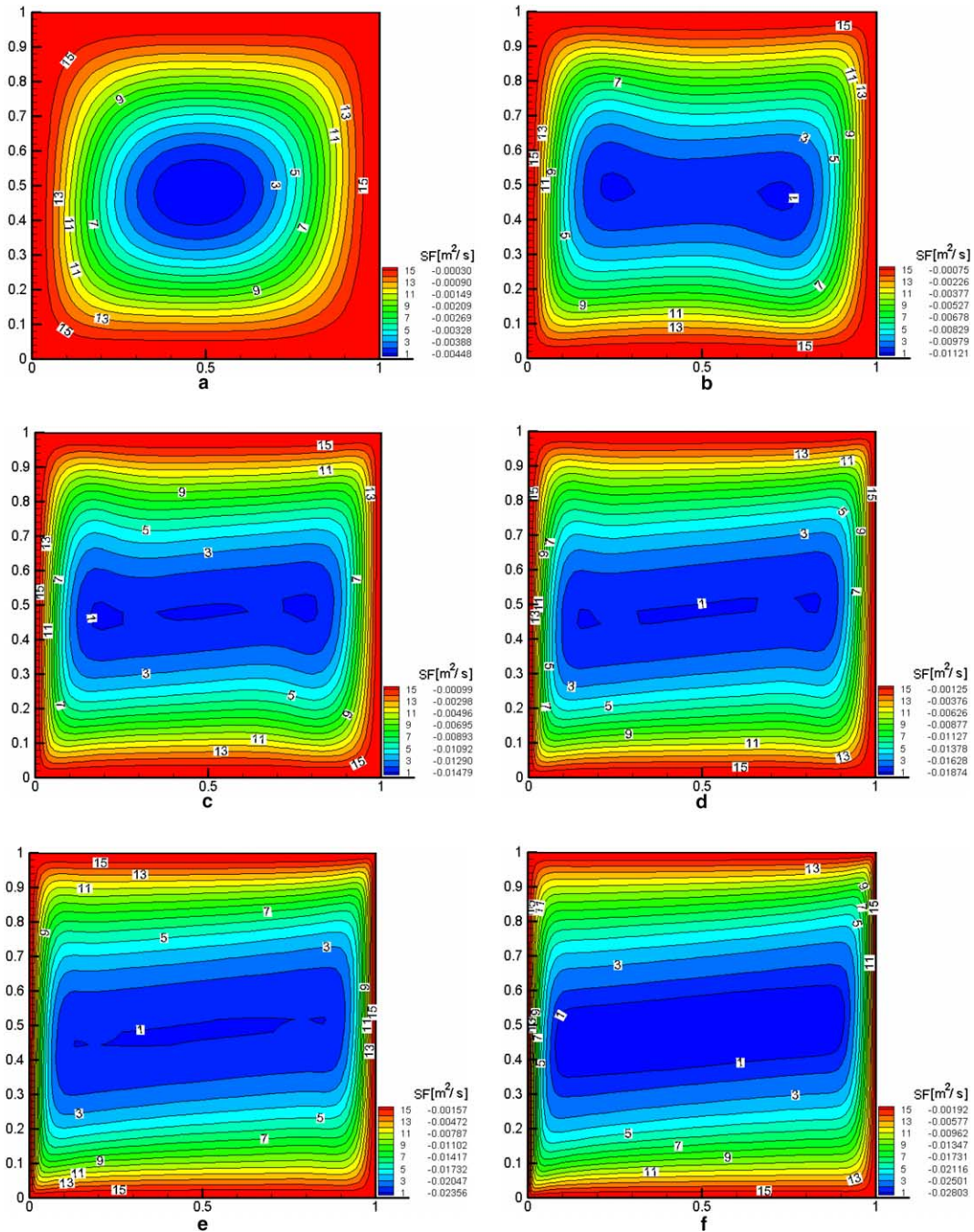


Fig. 5. Streamlines for a porous cavity with $\phi = 0.84$, $Pr = 1$, $k_s/k_f = 1$, $Re_m = 10^4$: (a) $Da = 1$, $\phi = 0.998$, (b) $Da = 0.3087 \times 10^{-1}$, (c) $Da = 0.7717 \times 10^{-2}$, (d) $Da = 1.929 \times 10^{-3}$, (e) $Da = 0.4823 \times 10^{-3}$ and (f) $Da = 1.206 \times 10^{-4}$.

continuum approach raises Nu by $(32.94 - 32.87)/32.87 \times 100 = +0.2\%$ for $N = 4$ and $(70.8 - 66.7)/66.7 \times 100 = +6\%$ for $N = 64$, which represents a much weaker influence of turbulence than in the case of Nu_ϕ . Therefore, one can infer that for $Re_m = 10^6$ the flow is

already fully turbulent because results using only laminar model solution gives average Nusselt numbers lower than those obtained with the turbulent model solution.

Fig. 7 further shows results using the turbulent model solution for: (a,b) streamlines, (c,d) isotherms,

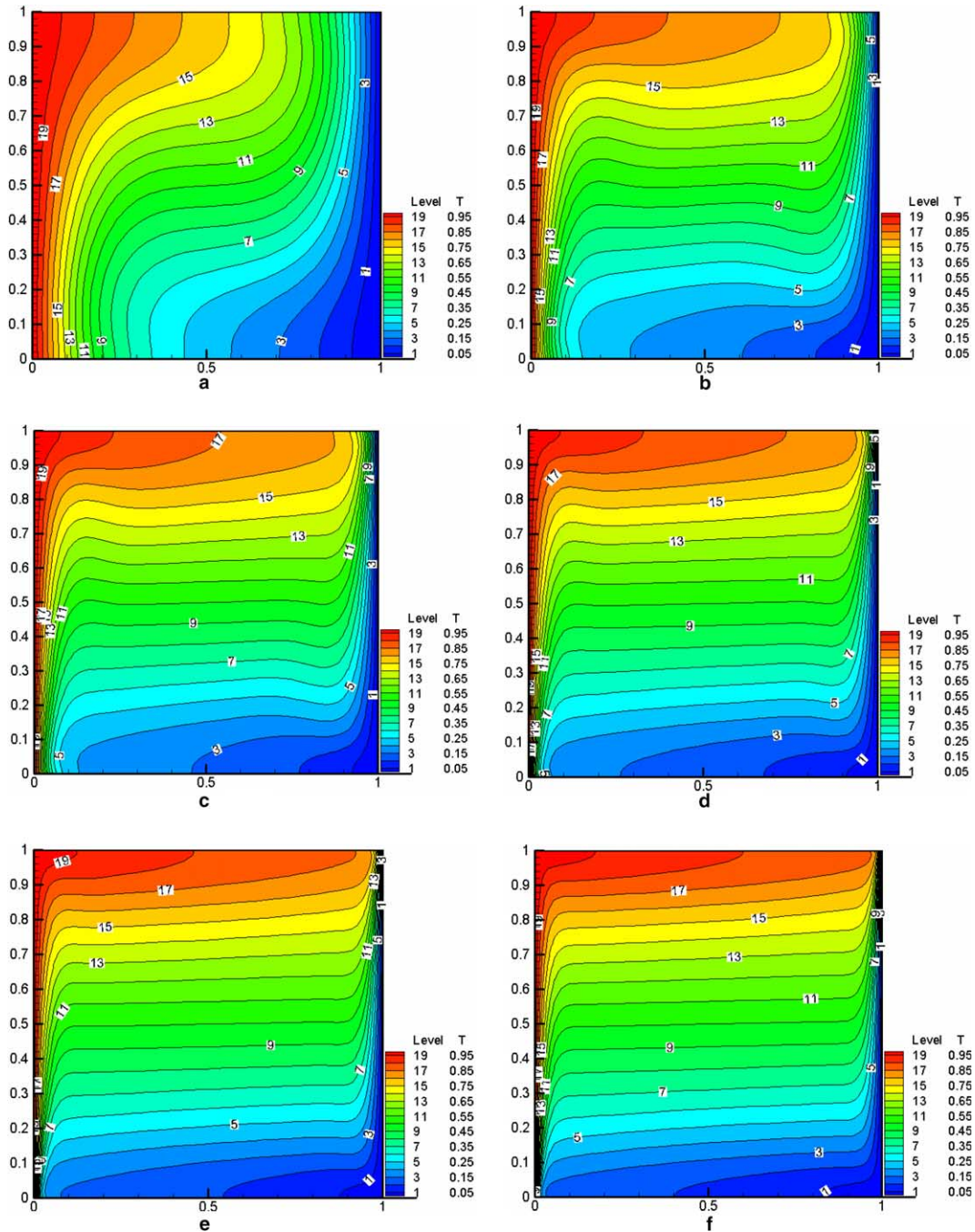


Fig. 6. Isotherms for a porous cavity with $\phi = 0.84$, $Pr = 1$, $k_s/k_f = 1$, $Ra_m = 10^4$: (a) $Da = 1$, $\phi = 0.998$, (b) $Da = 0.3087 \times 10^{-1}$, (c) $Da = 0.7717 \times 10^{-2}$, (d) $Da = 1.929 \times 10^{-3}$, (e) $Da = 0.4823 \times 10^{-3}$ and (f) $Da = 1.206 \times 10^{-4}$.

(e,f) Isolines of turbulent kinetic energy, k , for $\phi = 0.84$, $Ra_m = 10^6$, $Da = 0.4823 \times 10^{-3}$, $k_s/k_f = 1$, $Pr = 1$ for *continuum* and *porous-continuum* model respectively. Fig. 7a presents some recirculations between the solid obstacles and that recirculations are turbulent kinetic

energy generators in such regions, see Fig. 7e. Nevertheless, the flow pattern for the two models considered show satisfactory agreement when qualitatively compared, see Fig. 7a and b. As mentioned, the porous-continuum model seems to be more representative of reality

Table 4
Average Nusselt number for buoyancy-driven laminar flow in porous cavities

Ra_m	10	10^2	10^3	10^4
Walker and Homsy, 1978 [4]	–	3.097	12.96	51.0
Bejan, 1979 [5]	–	4.2	15.8	50.8
Beckerman, 1986 [7]	–	3.113	–	48.9
Gross et al, 1986 [8]	–	3.141	13.448	42.583
Manole and Lage, 1992 [9]	–	3.118	13.637	48.117
Moya et al, 1987 [10]	1.065	2.801	–	–
Baytas and Pop, 1999 [13]	1.079	3.16	14.06	48.33
Braga and de Lemos, 2004 [32], $Da = 10^{-8}$, $Pr = 1$	1.0908	3.0979	13.2751	43.5799

Table 5
Laminar and turbulent average Nusselt number for the continuum and porous-continuum models for $0.7717 \times 10^{-2} < Da < 0.4823 \times 10^{-3}$ and $Pr = 1$, $\phi = 0.84$, $Ra_m = 10^6$ and $k_s/k_f = 1$

$Da = Da_{eq}$	Laminar model solution		Turbulent model solution		
	Nu	Nu_ϕ	Nu	Nu_ϕ	N
0.7717×10^{-2}	32.8734	27.7820	32.9399	30.7346	4
1.9290×10^{-3}	46.4907	36.7713	46.6804	43.7739	16
0.4823×10^{-3}	66.6977	48.3144	70.7901	62.1561	64

when the number of obstacles inside the cavity is large, which, in turn, correspond to lower permeability cases.

Fig. 7c shows some peeks in the isotherms when compared with the isotherms from the Fig. 7d. This distortion on the thermal field is a response of the system due to the non-homogeneity of the heat mixing process. However, both models show a stratificated thermal field, see Fig. 7c and d.

Fig. 7e shows the isolines of k for the *continuum* model solution and one can note that the steepest velocity gradients are found near to the heated walls and between the solid obstacles. For that reason the generation of turbulent kinetic energy is considerably higher in such regions. On the other hand, the *porous-continuum* approach, Fig. 7f, show a high turbulent kinetic energy generation only close to the heated wall while the center of the cavity does not contribute to the k generation.

5.4. Nusselt number

Finally, Fig. 8 compares the behavior of the average Nusselt number for the two models here investigated, namely the *porous-continuum* and *continuum* models. Both calculation methods were based on the same numerical values for both the Rayleigh and the Darcy numbers. It is clearly seen in the figure that, if $Ra = Ra_\phi$ and $Da_{eq} = Da$ for both models, the overall values of average Nusselt number for the porous-continuum, Nu_ϕ model are lower than those obtained with the continuum model, Nu . This difference increases, with increasing number of rods N . Therefore, the porous-

continuum model fails in predicting the average Nusselt number, when compared with those obtained from the continuum model with several obstacles.

A possible explanation for such discrepancy is twofold: First, similar cases for the porous and porous-continuum models were compared under the condition $Ra_\phi = Ra$ (or $\beta_\phi = \beta$). However, it has already been pointed out in de Lemos and Braga [31] that these two thermal expansion coefficients do not, necessarily, have equal values. In fact, expression (9), derived in [31], shows the relationship between these two parameters. The first one, β , is a fluid property and for an ideal gas it is given by $1/T$, where T is the absolute gas temperature. On the other hand, β_ϕ is a macroscopic quantity, defined in Eq. (9), and by no means represents a local fluid property. Consequently, comparisons with the two models here investigated on the basis $\beta_\phi = \beta$ are strictly not quite correct. For having the same Nu , a inspection in Fig. 8 indicates that one should have $Ra_\phi > Ra$ when comparing the two models.

Secondly, both models were compared in Fig. 8 using the same value for parameter Darcy, or $Da_{eq} = Da$. Note that Da_{eq} is an “equivalent” Darcy number, whose associated K_{eq} in the continuum model was estimated by (14), being D_p the rod size. On the other hand, Da is the Darcy number for the porous cavity of Fig. 1d formed with the porous medium permeability K . In the simulation herein, the same K_{eq} value was prescribed in the porous-continuum model for use in Eq. (4), or say, $K_{eq} = K$. However, Eq. (14) was derived for forced convection flow over a porous bed so that its application to

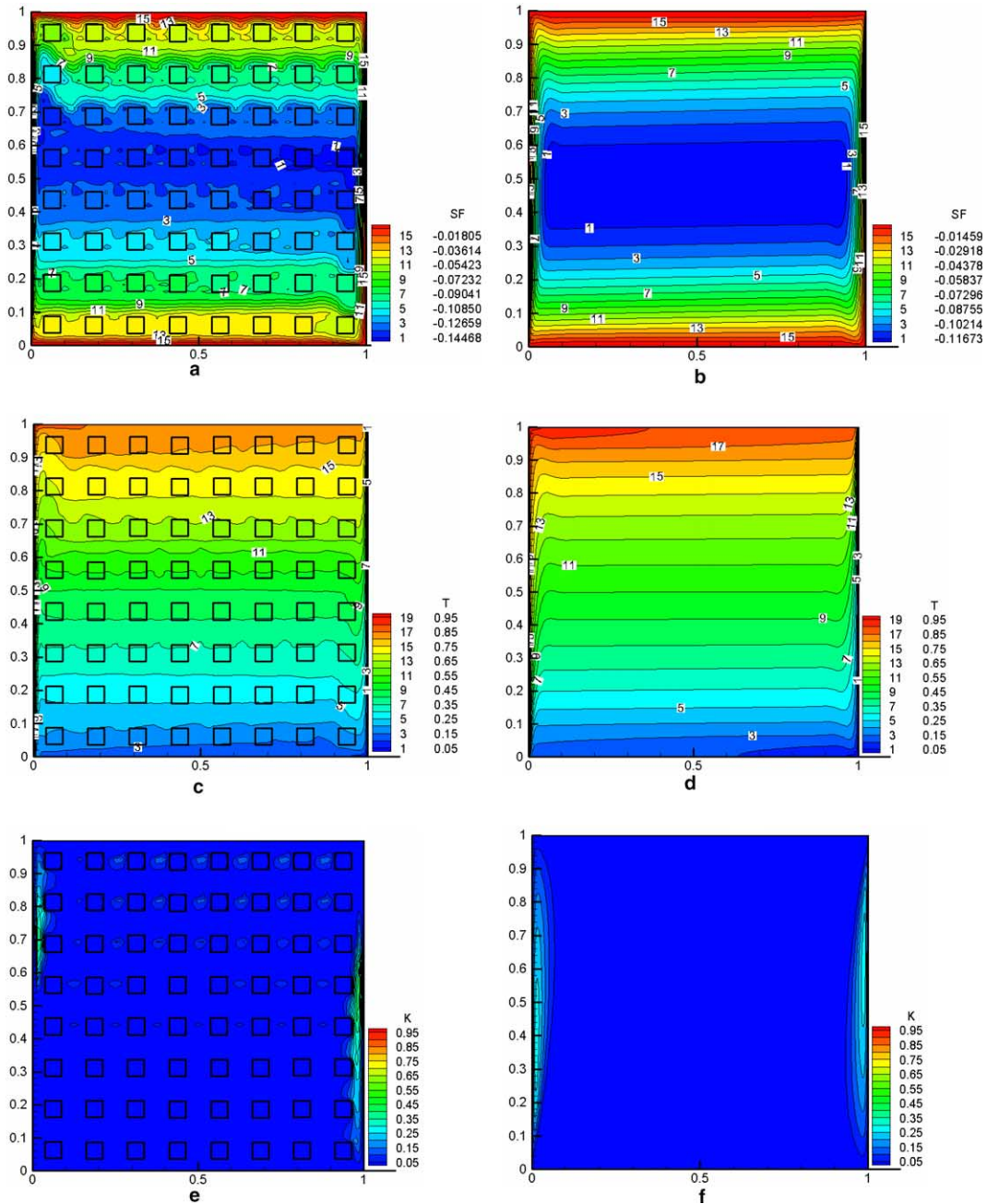


Fig. 7. Turbulent model solution using the continuum (left) and porous-continuum (right) models for $\phi = 0.84$, $Ra_m = 10^6$, $Da = 0.4823 \times 10^{-3}$, $k_s/k_f = 1$, $Pr = 1$: (a,b) streamlines, (c,d) isotherms, (e,f) isolines of turbulent kinetic energy, k .

the natural convection problem here under analysis is questionable. Also, real porous systems like the ones in Fig. 1a may have lower permeability than those associated with their counterpart continuum models of Fig. 1b. As the number of rods, N , increases, K_{eq} associated with Fig. 1b the might be reduced at a rate faster than that given by Eq. (14). So, when calculating a coun-

terpart porous-continuum model for the system in Fig. 1b, a lower value for K should be used instead of K_{eq} given by Eq. (14), or say, $Da < Da_{eq}$.

Therefore, in order to try to match Nusselt numbers calculated with both models here described, a correction is applied to the values given by the porous-continuum model. This correction is set by first curve fitting the

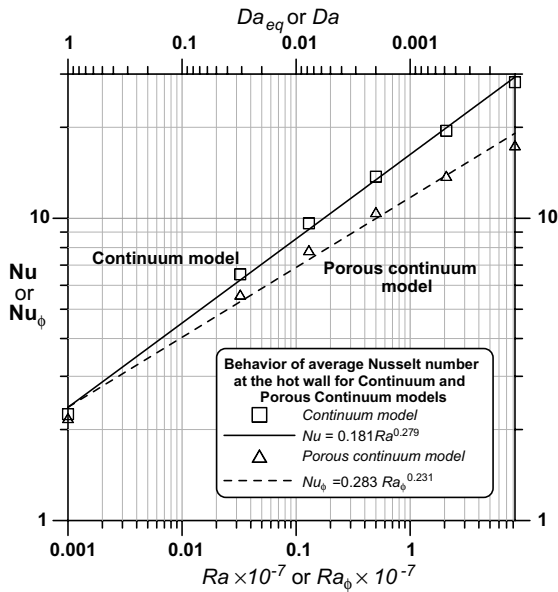


Fig. 8. Comparison between the continuum and porous-continuum models with respect to the average Nusselt number at the hot wall.

values of Nu in Fig. 8. For the two models applied, the following curves result

$$Nu = 0.181Ra^{0.279} \tag{19}$$

$$Nu_\phi = 0.283Ra_\phi^{0.231} \tag{20}$$

where Eqs. (19) and (20) refer to fitting curves obtained from the points of the average Nu (symbols) calculated with continuum and porous-continuum models, respectively. Now, by combining these two fittings, namely Eqs. (19) and (20), one yields the following expression:

$$Ra_\phi = 0.144Ra^{1.208} \tag{21}$$

As such, for matching Nu calculated from the two models, namely continuum and porous-continuum models, Ra_ϕ given by (21) should be used instead of $Ra_\phi = Ra$. Also, keeping all parameters the same in Eqs. (11) and (13), correction (21) is equivalent to setting $\beta_\phi = 4.128\beta^{1.208}$. This correction means that for calcu-

lating equivalent Nu with both models, one has to have $Ra_\phi > Ra$.

Further, in order to keep,

$$Ra_m = \underbrace{Ra_\phi Da}_{\text{Porous-continuum model}} = \underbrace{Ra Da_{eq}}_{\text{Continuum model}} = 10^4 \tag{22}$$

a relationship between the two Darcy numbers was also considered. Using Eq. (21) under the constraint (22) yields for such connection,

$$Da = 1.005Da_{eq}^{1.208} \tag{23}$$

which is equivalent to having $K = 1.005K_{eq}^{1.208}$ since $Da = K/H^2$ and Da_{eq} is defined in Eq. (15).

Therefore, in addition to using (21) for matching the Nusselt numbers given by the two models, which are represented by the correlations (19) and (20), one has also to use (23) instead of applying $Da = Da_{eq}$.

After that, new runs were performed for the porous-continuum model using now a macroscopic Rayleigh number given by (21), instead of using $Ra_\phi = Ra$, with corresponding Darcy numbers expressed by (23), used in place of $Da = Da_{eq}$. These new runs were performed while Ra_m was kept constant in such a way that

$$Ra_m = \underbrace{Ra_\phi Da}_{\text{Using } Ra_\phi=Ra, Da=Da_{eq}} = \underbrace{Ra_\phi Da}_{\text{Using Eqs. (21) and (23)}} = 10^4 \tag{24}$$

As a result, the use of (21) and (23) yielded corrected macroscopic Nusselt numbers, $Nu_{\phi,corr}$. Table 6 shows average values of Nusselt numbers for the continuum (Nu), porous-continuum with $Ra_\phi = Ra$ and $Da = Da_{eq}$ (Nu_ϕ) and corrected porous-continuum using (21) and (23) ($Nu_{\phi,corr}$). The percent errors shown in the table are calculates as,

$$\varepsilon = \frac{Nu_\phi - Nu}{Nu} \times 100; \quad \eta = \frac{Nu_{\phi,corr} - Nu}{Nu} \times 100 \tag{25}$$

According to Table 6, the overall values of the corrected average Nusselt numbers $Nu_{\phi,corr}$ are still lower than those obtained from the continuum model for

Table 6

Average Nusselt number for the continuum, porous-continuum and corrected porous-continuum models for Da ranging from 1 to 1.206×10^{-4} and $Pr = 1$, $\phi = 0.84$, $Ra_m = 10^4$, $k_s/k_f = 1$

N	Da	Nu	Nu_ϕ	$Nu_{\phi,corr}$	ε (%)	η (%)
0	1	2.2493	2.1854	2.1834	-2.84	-2.93
1	0.3087×10^{-1}	6.5254	5.5960	6.6804	-14.24	2.37
4	0.7717×10^{-2}	9.6204	7.8484	9.7677	-18.42	1.53
16	1.9290×10^{-3}	13.7276	10.4911	13.3775	-23.57	-2.55
64	0.4823×10^{-3}	19.4821	13.8199	17.9348	-29.06	-7.94
256	1.2060×10^{-4}	28.2085	17.4460	22.8239	-38.15	-19.08

lower Da numbers or for cases with N large. Nevertheless, as can be seen in the table, η values are substantially lower in comparison with ε . One should point out that thermal dispersion was not considered in this work and that this additional mixing mechanism might be important for cases with a large number of blocks, which correspond to cases in Table 6 presenting the largest discrepancies between the continuum and porous-continuum solutions, even with the corrections on Nu obtained with the use of Eqs. (21) and (23).

In the end, when results herein are seen along with those presented in Ref. [32], which used the porous-continuum model for simulating macroscopic turbulent flow in heated cavities with dispersion, there seems to be an indication that inclusion of turbulence and dispersion as additional exchange mechanisms is mandatory to reflect the actual heat transfer rate across the cavity, particularly for cases with large N . Ultimately, a more realistic macroscopic model, accounting for all possible mechanisms, will result in macroscopic values for Nu_ϕ that will be closer to microscopic computations of Nu , making cheaper and easy-to-implement macroscopic models a suitable engineering tool for analyzing complex physical systems as the ones in Fig. 1a.

6. Conclusions

This work presented numerical solutions for steady laminar and turbulent natural convection within a square cavity filled by a fixed amount of conducting solid material using a *continuum* model. The solid phase was composed by square obstacles, equally spaced within the cavity. In addition, an isotropic and homogeneous *porous-continuum* model was used for simulating the flow and heat transfer across the cavity, assuming the enclosure as totally filled with a porous material. The main conclusions of this work are:

- (1) The *porous-continuum* model failed to correctly predict the average Nusselt number when compared with those obtained from the *continuum* model with several obstacles. This same conclusion has also been reached in the recent literature [44].
- (2) An adjustment for the Rayleigh and Darcy numbers associated with the macroscopic model was proposed in order to match the average Nusselt number computed by the two approaches for a fixed $Ra_m = 10^4$. After such correction, the overall values of the corrected average Nusselt numbers were still lower than those obtained from the continuum model, mostly for the lower Da numbers cases, which correspond to cases with greater number of blocks N .

- (3) Both the *continuum* and the *porous continuum* models give higher values for the Nusselt number when turbulence is considered, being *macroscopic* solutions more sensitive to the inclusion of a turbulence model. This sensitivity increases with the number of blocks N .

Finally, results herein indicate that inclusion of turbulence and dispersion construct more realistic macroscopic models, making them a suitable engineering tool for analyzing complex physical systems.

Acknowledgement

The authors are thankful to CNPq and FAPESP, Brazil, for their financial support during the course of this research.

References

- [1] H. Bénard, Les tourbillons cellulaires dans une nappe liquide transportant de la chaleur par convection en régime permanent, Ann. Chim. Phys. 23 (1901) 62–144.
- [2] L. Rayleigh (J.W. Strutt), On convection currents in a horizontal layer of fluid when the higher temperature is on the underside, Philos. Mag. 32 (6) (1926) 833–844.
- [3] G. de Vahl Davis, Natural convection in a square cavity: A benchmark numerical solution, Int. J. Numer. Methods Fluids 3 (1983) 249–264.
- [4] K.L. Walker, G.M. Homsy, Convection in porous cavity, J. Fluid Mech. 87 (1978) 449–474.
- [5] A. Bejan, On the boundary layer regime in a vertical enclosure filled with a porous medium, Lett. Heat Mass Transfer 6 (1979) 93–102.
- [6] V. Prasad, F.A. Kulacki, Convective heat transfer in a rectangular porous cavity-effect of aspect ratio on flow structure and heat transfer, J. Heat Transfer 106 (1984) 158–165.
- [7] C. Beckermann, R. Viskanta, S. Ramadhyani, A numerical study of non-Darcian natural convection in a vertical enclosure filled with a porous medium, Numer. Heat Transfer 10 (1986) 557–570.
- [8] R.J. Gross, M.R. Bear, C.E. Hickox, The application of flux-corrected transport (FCT) to high Rayleigh number natural convection in a porous medium, in: Proceedings of 8th International Heat transfer Conference, San Francisco, CA, 1986.
- [9] D.M. Manole, J.L. Lage, Numerical benchmark results for natural convection in a porous medium cavity, HTD-Vol 216, Heat and mass Transfer in Porous Media, ASME Conference, 1992, pp. 55–60.
- [10] S.L. Moya, E. Ramos, M. Sen, Numerical study of natural convection in a tilted rectangular porous material, Int. J. Heat Mass Transfer 30 (1987) 741–756.
- [11] D.A. Nield, A. Bejan, Convection in Porous Media, Springer, New York, 1992.

- [12] D.B. Ingham, I. Pop, *Transport Phenomena in Porous Media*, Elsevier, Amsterdam, 1998.
- [13] A.C. Baytas, I. Pop, Free convection in oblique enclosures filled with a porous medium, *Int. J. Heat Mass Transfer* 42 (1999) 1047–1057.
- [14] C.T. Hsu, P. Cheng, Thermal dispersion in a porous medium, *Int. J. Heat Mass Transfer* 33 (1990) 1587–1597.
- [15] J. Bear, *Dynamics of Fluids in Porous Media*, American Elsevier Pub. Co., New York, 1972.
- [16] S. Whitaker, Equations of motion in porous media, *Chem. Eng. Sci.* 21 (1966) 291–300.
- [17] S. Whitaker, Diffusion and dispersion in porous media, *J. Am. Inst. Chem. Eng.* 13 (3) (1967) 420–427.
- [18] T. Masuoka, Y. Takatsu, Turbulence model for flow through porous media, *Int. J. Heat Mass Transfer* 39 (13) (1996) 2803–2809.
- [19] F. Kuwahara, A. Nakayama, H. Koyama, A numerical study of thermal dispersion in porous media, *J. Heat Transfer* 118 (1996) 756–761.
- [20] F. Kuwahara, A. Nakayama, Numerical modeling of non-Darcy convective flow in a porous medium, in: *Heat Transfer 1998: Proceedings of 11th International Heat Transfer Conference Kyongyu Korea*, 4, Taylor & Francis, Washington, DC, 1998, pp. 411–416.
- [21] F. Kuwahara, Y. Kameyama, S. Yamashita, A. Nakayama, Numerical modeling of turbulent flow in porous media using a spatially periodic array, *J. Porous Media* 1 (1) (1998) 47–55.
- [22] K. Lee, J.R. Howell, Forced convective and radiative transfer within a highly porous layer exposed to a turbulent external flow field, in: *Proceedings of the 1987 ASME–JSME Thermal Engineering Joint Conference*, Honolulu, Hawaii, 2, ASME, New York, NY, 1987, pp. 377–386.
- [23] B.V. Antohe, J.L. Lage, A general two-equation macroscopic turbulence model for incompressible flow in porous media, *Int. J. Heat Mass Transfer* 40 (13) (1997) 3013–3024.
- [24] D. Getachewa, W.J. Minkowycz, J.L. Lage, A modified form of the k - ϵ model for turbulent flow of a incompressible fluid in porous media, *Int. J. Heat Mass Transfer* 43 (2000) 2909–2915.
- [25] M.H.J. Pedras, M.J.S. deLemos, On the definition of turbulent kinetic energy for flow in porous media, *Int. Commun. Heat Mass Transfer* 27 (2) (2000) 211–220.
- [26] M.H.J. Pedras, M.J.S. de Lemos, Macroscopic turbulence modeling for incompressible flow through undeformable porous media, *Int. J. Heat Mass Transfer* 44 (6) (2001) 1081–1093.
- [27] M.H.J. Pedras, M.J.S. de Lemos, Simulation of turbulent flow in porous media using a spatially periodic array and a low-re two-equation closure, *Numer. Heat Transfer—Part A Appl.* 39 (1) (2001) 35–59.
- [28] M.H.J. Pedras, M.J.S. de Lemos, On the mathematical description and simulation of turbulent flow in a porous medium formed by an array of elliptic rods, *J. Fluids Eng.* 123 (4) (2001) 941–947.
- [29] F.D. Rocamora Jr., M.J.S. de Lemos, Analysis of convective heat transfer of turbulent flow in saturated porous media, *Int. Commun. Heat Mass Transfer* 27 (6) (2000) 825–834.
- [30] M.J.S. de Lemos, F.D. Rocamora, Turbulent transport modeling for heated flow in rigid porous media, in: *Proceedings of the Twelfth International Heat Transfer Conference*, Grenoble, France, August 18–23, 2002, pp. 791–795.
- [31] M.J.S. de Lemos, E.J. Braga, Modeling of turbulent natural convection in saturated rigid porous media, *Int. Commun. Heat Mass Transfer* 30 (5) (2003) 615–624.
- [32] E.J. Braga, M.J.S. de Lemos, Turbulent natural convection in a porous square cavity computed with a macroscopic k - ϵ model, *Int. J. Heat Mass Transfer* 47 (26) (2004) 5639–5650.
- [33] M.J.S. de Lemos, M.S. Mesquita, Turbulent mass transport in saturated rigid porous media, *Int. Commun. Heat Mass Transfer* 30 (1) (2003) 105–113.
- [34] M. Saito, M.J.S. de Lemos, Interfacial heat transfer coefficient for non-equilibrium convective transport in porous media, *Int. Commun. Heat Mass Transfer* 32 (5) (2005) 667–677.
- [35] M.J.S. de Lemos, L.A. Tofaneli, Modeling of double-diffusive turbulent natural convection in porous media, *Int. J. Heat Mass Transfer* 47 (19–20) (2004) 4221–4231.
- [36] M.J.S. de Lemos, M.H.J. Pedras, Recent mathematical models for turbulent flow for saturated rigid porous media, *J. Fluids Eng.* 123 (4) (2001) 935–940.
- [37] R.A. Silva, M.J.S. de Lemos, Numerical analysis of the stress jump interface condition for laminar flow over a porous layer, *Numer. Heat Transfer Part A—Appl.*, USA 43 (6) (2003) 603–617.
- [38] R.A. Silva, M.J.S. de Lemos, Turbulent flow in a channel occupied by a porous layer considering the stress jump at the interface, *Int. J. Heat Mass Transfer* 46 (26) (2003) 5113–5121.
- [39] M.J.S. de Lemos, Turbulent kinetic energy distribution across the interface between a porous medium and a clear region, *Int. Commun. Heat Mass Transfer* 32 (1–2) (2005) 107–115.
- [40] J.M. House, C. Beckermann, T.F. Smith, Effect of a centered conducting body on natural heat transfer in a enclosure, *Numer. Heat Transfer A* 18 (1990) 213–225.
- [41] A.A. Merrikh, A.A. Mohamad, Blockage effects in natural convection in differentially heated enclosures, *J. Enhanced Heat Transfer* 8–1 (2001) 55–72.
- [42] A.A. Merrikh, J.L. Lage, A.A. Mohamad, Comparison between pore-level and porous medium models for natural convection in a non-homogeneous enclosure, fluid flow and transport in porous media: mathematical and numerical treatment, in: Z. Chen, R. Erwin (Eds.), *Contemporary Mathematics*, vol. 295 (2002) 387–396.
- [43] A.A. Merrikh, J.L. Lage, A.A. Mohamad, Natural convection in non-homogeneous heat generating media: Comparison of continuum and porous-continuum models, *J. Porous Media* 8 (2) 149–163.
- [44] N. Massarotti, P. Nithiarasu, A. Carotenuto, Microscopic and macroscopic approach for natural convection in enclosures filled with fluid saturated porous medium, *Int. J. Numer. Meth. Heat Fluid Flow* 13 (7) (2003) 862–886.
- [45] A.A. Merrikh, J.L. Lage, Effect of distributing a fixed amount of solid constituent inside a porous medium enclosure on the heat transfer process, in: *ICAPM*

- 2004—Proceedings of International Conference on Applications of Porous Media, 2004, pp. 51–57.
- [46] A.A. Merrikh, J.L. Lage, Natural convection in a enclosure with disconnected and conducting solid blocks, *Int. J. Heat Mass Transfer* 48 (7) (2005) 1361–1372.
- [47] A. Nakayama, F. Kuwahara, A macroscopic turbulence model for flow in a porous medium, *J. Fluids Eng.* 121 (1999) 427–433.
- [48] S. Ergun, Fluid flow through packed columns, *Chem. Eng. Process* 48 (1952) 89–94.
- [51] S.V. Patankar, D.B. Spalding, A calculation procedure for heat, mass and momentum transfer in three dimensional parabolic flows, *Int. J. Heat Mass Transfer* 15 (1972) 1787.
- [52] H.L. Stone, Iterative solution of implicit approximations of multi-dimensional partial differential equations, *SIAM J. Numer. Anal.* 5 (1968) 530–558.
- [53] A.A. Merrikh, A.A. Mohamad, Non-Darcy effects in buoyancy driven flows in an enclosures filled with vertically layered porous media, *Int. J. Heat Mass Transfer* 45 (2002) 4305–4313.
- [54] J.C. Kalita, D.C. Dalal, A.K. Dass, Fully compact higher-order computation of steady state natural convection in a square cavity, *Phys. Rev. E* 64-066703 (2001) 1–13.
- [55] J.L. Lage, A. Bejan, The Ra-Pr domain of laminar natural convection in an enclosure heated from the side, *Numer. Heat Transfer A* 19 (1991) 21–41.